RSC Advances

PAPER

View Article Online
View Journal | View Issue

Cite this: *RSC Adv.*, 2019, **9**, 15772

The aggression behavior study of Cl^- on the defect structure of passive films on copper

Aoni Xu,[ab] Chaofang Dong,*[a] Xin Wei,[a] Xiaogang Li[a] and Digby D. Macdonald[b]

The destructive role of chloride ions on the defect structure of barrier layers (bl) is vitally important for understanding the initial breakdown of passive films on metals. Here photo-electrochemical and density functional theory (DFT) were applied to investigate the influence of chloride on the defect structure of the bl in passive films. The results show a bl with a narrow band gap, in which the valence band maximum (VBM) increased upon introducing chloride into the electrolyte. DFT calculations indicate that an increase in the copper vacancy concentration, due to cation extraction at the bl/solution interface could increase the VBM while oxygen vacancy generation results in a decrease in the conduction band minimum (CBM). The combination of these results verifies the aggressive role of chloride as proposed by the Point Defect Model (PDM) where an enhancement of the cation vacancy concentration across the bl occurs in response to the absorption of Cl^- into oxygen vacancies on the bl.

Received 6th May 2019
Accepted 15th May 2019

DOI: 10.1039/c9ra03402a

rsc.li/rsc-advances

1. Introduction

Copper generally exhibits excellent chemical stability under oxidizing conditions in contact with aqueous solutions owing to the formation of a thin oxide film that is only a few nanometers thick. Unfortunately, in spite of having this self-protective function, copper still suffers serious damage in some highly aggressive environments.[1–3] Early investigations[4–7] established the susceptibility of Cu to pitting corrosion resulting from the rapid breakdown of the protective film in aqueous halide solutions, especially in chloride-containing solutions. The overall reaction can be written as: $\frac{1}{2}Cu_2O(s) + 2Cl^- + H^+ \rightarrow CuCl_2^- + \frac{1}{2}H_2$[8] However, the role of highly defective structure of the passive film should not be neglected when we discuss the detailed mechanism of chloride ion-induced breakdown. Our previous work[9] has demonstrated that the breakdown of passive films on copper in chloride solution is due to the adsorption behavior rather than the penetration of Cl^- into the barrier oxide layer (bl) by both experiment and Density Functional Theory (DFT) calculations. A further investigation should be performed aimed at the detailed process of initial breakdown of the passive film induced by adsorbed chloride ions in solution. It is evident that the point defect structure of the bl is vitally important in understanding the physico-electrochemistry of passivity breakdown on metals and alloys.[10] Thus, how the chloride ions impact the defect structure of passive film would be crucial to understand the initial breakdown. Not surprisingly, this has led many workers to examine the defect structure of bls using a variety of techniques.[11–13] However, the defect structure of a barrier layer is difficult to define directly using conventional methods, such as photoluminescence excitation[14] and positron annihilation spectroscopy (PAS),[15] since the bl of a passive film is generally so thin (1–10 nm) that it is impossible to separate its response from that of the metal substrate. In past studies, researchers usually measured the carrier concentration in passive film using Mott–Schottky analysis (MSA) and used the results to reflect upon the variation of the point defect concentration.[16–19] Nevertheless, the value of point defect concentration in the bl, as determined by MSA, is problematic, as noted elsewhere,[20] and the relationship between point defect and carrier (electron and hole) concentrations is not well-defined because a lack of confluence between Mott–Schottky theory and the bl, which is not a simple p–n junction. Fortunately, the variation of the band structure also could reflect the change in the point defect concentration, since the point defects act as the dopants. Taking cuprous oxide (Cu_2O) as an example, Paul *et al.*[21] pointed out that the presence of copper vacancy could introduce hole states located on about 0.45 eV above the valence band maximum (VBM) in the band structure.

Furthermore, exploring the relationship between point defects and electronic structure of material by first principle calculations to explain reaction mechanism or guide material design has been generally accepted and has made significant progress in recent years. Raebiger *et al.*[22] studied the formation enthalpies of copper vacancy (V_{Cu}) and oxygen interstice (O_i) using DFT and found that the cation deficiency of Cu_2O is accommodated mostly by Cu vacancies V_{Cu} rather than by

[a]*Corrosion and Protection Center, Key Laboratory for Corrosion and Protection (MOE), University of Science and Technology Beijing, Beijing 100083, China. E-mail: cfdong@ustb.edu.cn; Fax: +86-10-62334005; Tel: +86-10-62333931 extn 518*

[b]*Department of Material Science and Engineering, The University of California at Berkeley, Berkeley, CA 94720, USA*

oxygen interstitials O_i (that is, the stoichiometry of the bl is $Cu_{2-x}O$ rather than Cu_2O_{1+y}, both of which give Cu/O < 2). Thus, in this paper, we used photo-electrochemical spectra to measure the band gap and ultraviolet photoelectron spectroscopy (UPS) to assess the position of VBM relative to the Fermi level. In this way, a simplified band structure of passive film could be obtained. Furthermore, defective Cu_2O slab models were employed to simulate the barrier layer on copper. The characteristic band structures were identified for various kinds of point defects using HSE functional. Finally, a rational, theoretical explanation combined with experimental observation, was proposed to explain the effect of chloride on the defect structure of bl and hence for the occurrence of initial passivity breakdown.

2. Methods and material

2.1 Experiments

Electrochemical experiments were performed at ambient temperature (22 ± 2 °C) in a special, three-electrode cell containing two quartz windows for optical access. The working electrode, fabricated from a pure copper rod (99.99%), was mounted in epoxy resin with a 0.3 cm^2 area exposed to the electrolyte. A saturated calomel electrode (SCE) and a Pt plate were employed as the reference electrode (RE) and the counter electrode (CE), respectively. A solution of pH = 7.6 ± 0.02 was established with borate buffer ($Na_2B_4O_7 \cdot 10H_2O$ 99.5% and H_2BO_3 99.5% assay) reagent-grade sodium chloride (NaCl 99.5%). During the entire experimental time, continuous nitrogen sparging into electrochemical cells were performed to avoid contamination from atmospheric oxygen.

Potentiodynamic polarizations (PDP) were commenced in the negative-to-positive direction at a scan rate of 0.1667 mV s^{-1} after pre-performed cathodically polarization at −0.6 V *vs.* SCE. Subsequently, anodic polarization at 0.2 V in passivity range was performed for 24 h to generate a steady-state passive film. Then, the work functions of passive films were measured using a Thermo Scientific ESCALab 250Xi system employing UPS. The gas discharge lamp was used with admitted helium gas and the HeI (21.22 eV) emission line employed. In the meantime, we performed photo-electrochemical measurements using a 150 W xenon lamp and a 1200/mm grating monochromator just after anodic polarization. The photocurrent spectra were obtained by scanning the light wavelength in steps of 10 nm from 800 to 300 nm. All of the electrochemical and photo-electrochemical experiments were achieved on a Solartron Analytical Modulab photo-electrochemistry workstation.

2.2 Computational studies

HSE06 functional[23] was applied in all calculations to obtain more accurate descriptions of electronic properties, in which the value of the exact nonlocal exchange correlation was set as 0.325 according to our previous work.[24] Similarly, norm-conserving pseudopotentials (NCPP) were used to describe the interaction between electron and ion. For a cubic Cu_2O supercell, the plane-wave energy cutoff and *k*-point meshes were set as 520 eV and 4 × 4 × 4 respectively. Extensive tests have been carried out to ensure convergence when the total force on each ion was reduced to less than 0.01 eV $Å^{-1}$. Then, three 5-layer (3 × 3) Cu_2O unit cells with a 15 Å vacuum region were constructed for modeling Cu_2O (100), (110) and (111) surfaces as ultrathin passive film on copper. The surface energies and electronic properties of three different facets models were calculated after structure optimization. To estimate the contribution of point defects to the electronic structure, vacancies were created by removing Cu/O ions individually from Cu_2O slab, followed by structure optimization. Meanwhile, configurations with chloride ions inserting into surface oxygen vacancies were employed to investigate the breakdown effect of chloride ions (negative chloride ions have same charge with cation vacancies, thus, it's unreasonable that anions interact with cation vacancy). Finally, band structures and density of states (DOS) calculations were performed for these defective models using PWmat software.[25,26]

3. Results

3.1 Experimental results

Fig. 1(a) shows the potentiodynamic polarization curves of Cu in pH = 7.64 buffer solution containing chloride. Clearly, the passive range of copper in neutral solution was gradually narrowed as the chloride concentration increased. Even no passivity, as evidenced by the passive current higher than $\sim 10^{-5}$ A cm^{-2}, was observed in 1 M NaCl. Then 0.2 V, which lies within the passivity range of copper in all electrolytes, was chose to form the passive film. Photocurrent spectra relating to anodic passive films grown in various solutions were measured and are shown in Fig. 1(b). The photo-absorption coefficient, α, depends on the photon energy related to the band gap of samples:[27]

$$\alpha = A(h\nu - E_g)^n/h\nu \quad (1)$$

where A is a constant, E_g is the band-gap energy; n relates to the electron transition type of semiconductor, 1/2 for a direct transition and 2 for an indirect transition (Cu_2O, the main composition of the bl, is a direct transition semiconductor[28]). The photocurrent, i_{ph}, was demonstrated[29] to be linearly dependent on absorption coefficient, α. Therefore, as Fig. 1(b) insets showed, the band-gap value can be determined from an $(i_{ph}h\nu)^{1/2}$ or $(i_{ph}h\nu)^2$ *versus* $h\nu$ plot by extrapolating to $i_{ph} = 0$. This analysis indicates that the bl generated in non-chloride containing electrolyte at 0.2 V has a 1.95 eV bandgap, which is slightly lower than the band gap of crystalline cuprous oxide (2.1 eV).[30] For the electrolyte containing chloride, the bl has an obviously narrower band gap of 1.72 and 1.53 eV in 0.1 M and 0.5 M NaCl solutions, respectively. Moreover, we subjected the valence band (VB) edges of the bl grown in different electrolytes to UPS analysis. Fig. 1(c) shows all of the photoemission spectra for the VB of the bl. The energy of the VB edge was obtained by extrapolating the linear part of the absorption edge to its intersection with the baseline. The figure shows that the electron binding energies of the VB edges of the bl formed in chloride-containing neutral solutions are slightly higher than their Fermi levels by 0.83, 0.72 and 0.35 eV, respectively. These results, especially in 0.1 M NaCl and no chloride solutions, are

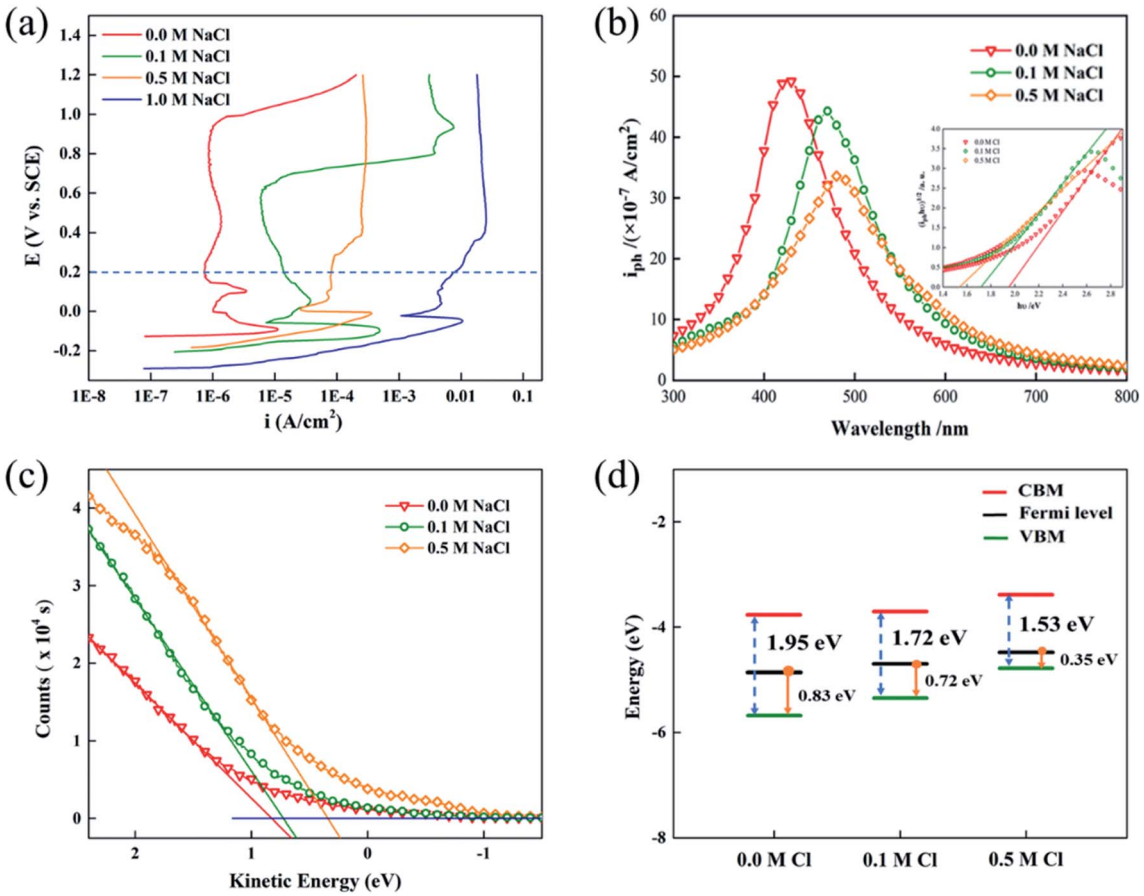

Fig. 1 (a) The anodic polarization curves of Cu in pH = 7.64 buffer solution and chloride-containing solution; (b) photocurrent spectra of passive film formed at 0.20 V; (c) photoemission spectra for the VB of passive film obtained from UPS analysis; (d) the band structure of passive film formed in various solutions, where CBM is conduction band minimum and VBM is valence band maximum.

consistent with the energy difference of the upper VB edge and the Fermi level of crystalline cuprous oxide (0.7 eV)[31] and previous work (0.8 eV).[32] The work functions of the bl were also measured by UPS. The value decreased with increasing chloride concentration; 4.86, 4.70 and 4.48 eV for 0, 0.1 and 0.5 M NaCl, respectively (Table 1).

Taking the results of band gap, position of the VBM, and work function into consideration, the band structures of the bl can be represented as Fig. 1(d). The bl of the passive film grown in 0.5 M NaCl had the narrowest band gap and the highest Fermi level (lowest work function), while the band gaps and Fermi levels were similar for the bls formed in two other solutions. Combining with the introducing of doping states by point defect, this change in band structure of passive film demonstrated that the chloride ions in electrolyte play a significant role in determining the defect structure of the bl by creating fresh vacancies. A similar increasing tendency of carrier density was also reported by Fattah-Alhosseini[33] by Mott–Schottky analysis. However, the interaction between chloride ions and the bl still lacks detail. Oxygen vacancies ($V_O^{\bullet\bullet}$) and cation vacancies (V'_{Cu}) in the bl, and even chloride absorbed into surface oxygen vacancies ($Cl_O^{\bullet}$) in bl, can all generate electronic doping states in the band gap, which renders the process difficult to be analyzed only from experiment. Thus, a more detailed analysis is warranted by using first-principles calculations.

Table 1 The surface energies and work function results of experiments and calculations

Experimental results		Calculation results	
Electrolyte	Work function/eV	Orientation	Surface energy/eV Å^{-2}
0.0 M NaCl	4.86	Cu_2O (100)	0.10
0.1 M NaCl	4.70	Cu_2O (110)	0.08
0.5 M NaCl	4.48	Cu_2O (111)	0.04

3.2 Calculational results

In this section, the most stable facet with lowest surface energy (Table 1), Cu_2O (111), which is also observed to be similar to that of the barrier layer of the passive film on copper by scanning tunneling microscope,[34] was used to study in detail the breakdown mechanism of chloride ions on the aspect of electronic properties.

On the most stable O-terminated Cu_2O (111) surface, 4 kinds of ions exist, named as Cu-1, Cu-2, O-3 and O-4 according to their coordination numbers [Fig. 2(g)]. We first investigated the surface work functions for complete and defective surface. For

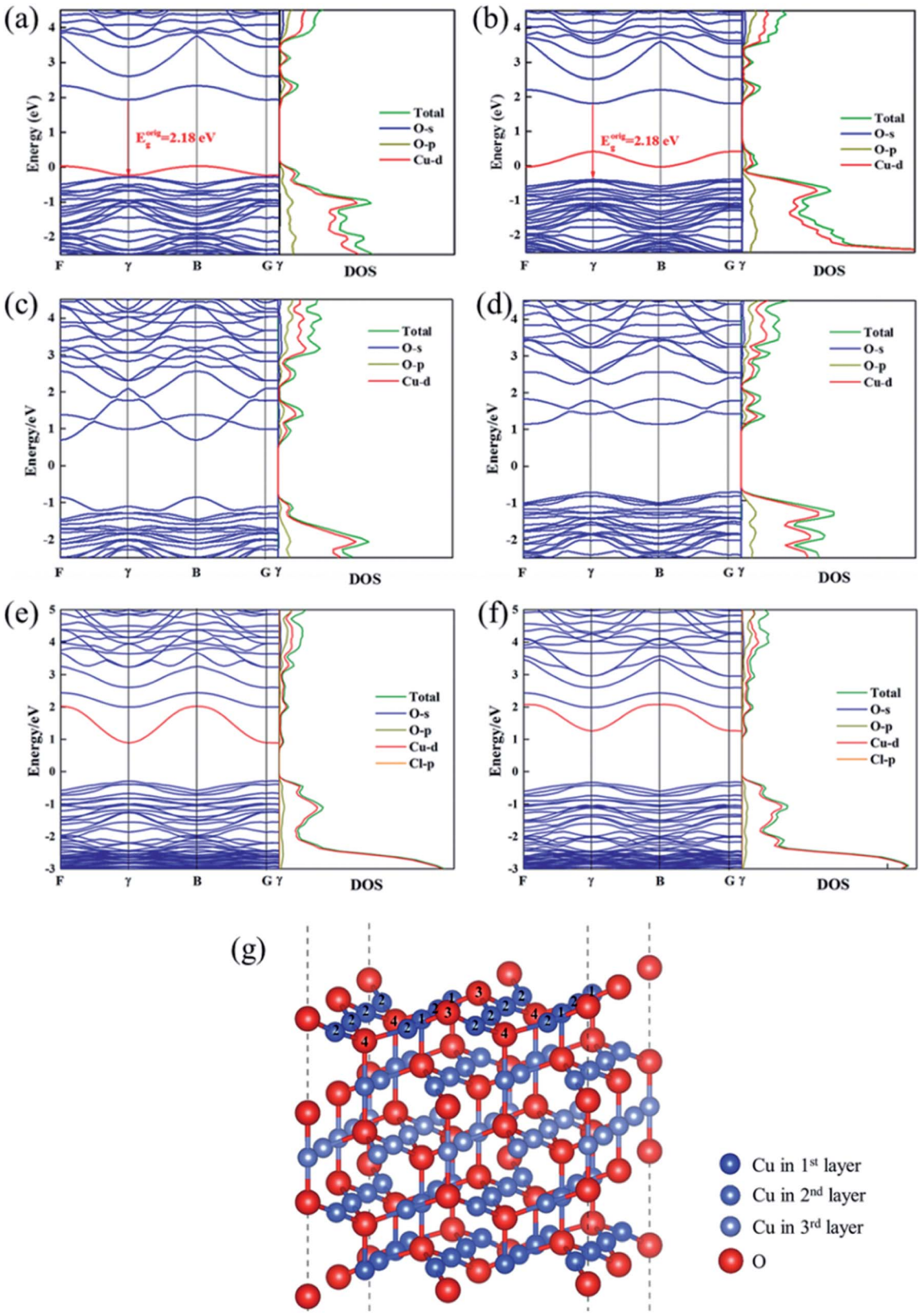

Fig. 2 Band structures and DOS of Cu_2O (111) with (a) $V'_{Cu\text{-}1}$; (b) $V'_{Cu\text{-}2}$; (c) $V^{\bullet\bullet}_{O\text{-}3}$; (d) $V^{\bullet\bullet}_{O\text{-}4}$; (e) $Cl^{\bullet}_{O\text{-}3}$; (f) $Cl^{\bullet}_{O\text{-}4}$; (g) side view of Cu_2O (111) slab model.

a perfect Cu_2O (111) surface, the work function equals to 4.87 eV which is very similar with our experimental result in Table 1. However, when we introduce surface point defect on our slab model, the work function values all decreased obviously where 4.77 and 4.75 eV for $V'_{Cu\text{-}1}$ and $V'_{Cu\text{-}2}$, 4.73 and 4.70 eV for $V^{\bullet\bullet}_{O\text{-}3}$ and $V^{\bullet\bullet}_{O\text{-}4}$, respectively. We also calculated the work function for the

adsorption model of chloride, where 5.04 and 5.35 eV for the configurations of Cl absorbed on Cu-1 and Cu-2. Therefore, a reasonable explanation for the decreasing work functions with increase in molarity of Cl observed in experiments was proposed "The barrier layer formed in a dense Cl-containing solution has a more defective structure". Furthermore, Fig. 2 displays the band structures and DOS of Cu_2O (111) with a copper or oxygen vacancies or an oxygen vacancy occupied by chloride. We have discussed the effect of cation vacancies on electronic properties and magnetic moments in detail in our previous work,[24] where O 2p and Cu 3d states dominate an additional acceptor state above VBM in band gap. On the contrary, for oxygen vacancies, especially Cl-occupied oxygen vacancies, a clear shift down of CBM was observed by introducing a donor state in the band gap [Fig. 2e and f]. Similarly, 3d states of copper atoms surrounding oxygen vacancy dominate the extension of the conduction band owing to the unsaturated dangling bonds appearing around the vacancy. The donor state introduced by Cl-occupied oxygen vacancy never changes the direct gap feature of stoichiometric Cu_2O compared with an unoccupied oxygen vacancy, which shifts the direct transition point in the Brillouin zone from Point γ- to Point B point for $V_{O\text{-}3}^{\cdot\cdot}$ and introduces an indirect gap for $V_{O\text{-}4}^{\cdot\cdot}$.

It should be noted that the real bl is inhomogeneous with gradients of the electric field and of the distribution of vacancies. Naturally, the field penetration and band bending must exist across the bls on metals owing the variational phase environment. However, it's almost impossible to create a model with the same distribution of vacancies and also electric field as a real passive film which is still a mystery on characterization experiments. Similarly, we have to be honest to say we cannot calculate the exact band structure of bl. But, we can apply the calculated electronic structure of cuprous oxide in a specific defective structure to analyze the effective role of a specific defect on electronic properties for bl by comparing calculation results of defective model and complete one. That's because the effective role of a specific vacancy for a semiconductor whether perfect or defective remains unchanged. Taking copper vacancy as an example, copper vacancy always acts as acceptor introducing hole states over valence band in band structure for Cu_xO ($1 < x < 2$).[22,35,36] To demonstrate that in detail, we also supplemented many electronic structure calculations under electric field of various values and with different defect concentrations.

Fig. 3 shows the band structures of Cu_2O (111) slab model with one $V'_{Cu\text{-}1}$ under 0, 1, 3 and 5×10^6 V cm^{-1} electric field. Meanwhile, the direction of applied electric field is parallel to z axis and the vacuum layer. As seen, the copper vacancy $V_{Cu\text{-}1}$ always acts as acceptor and introduce a shallow hole state above valence band no matter in which electric field. The electronic structures of cuprous oxide with different defect

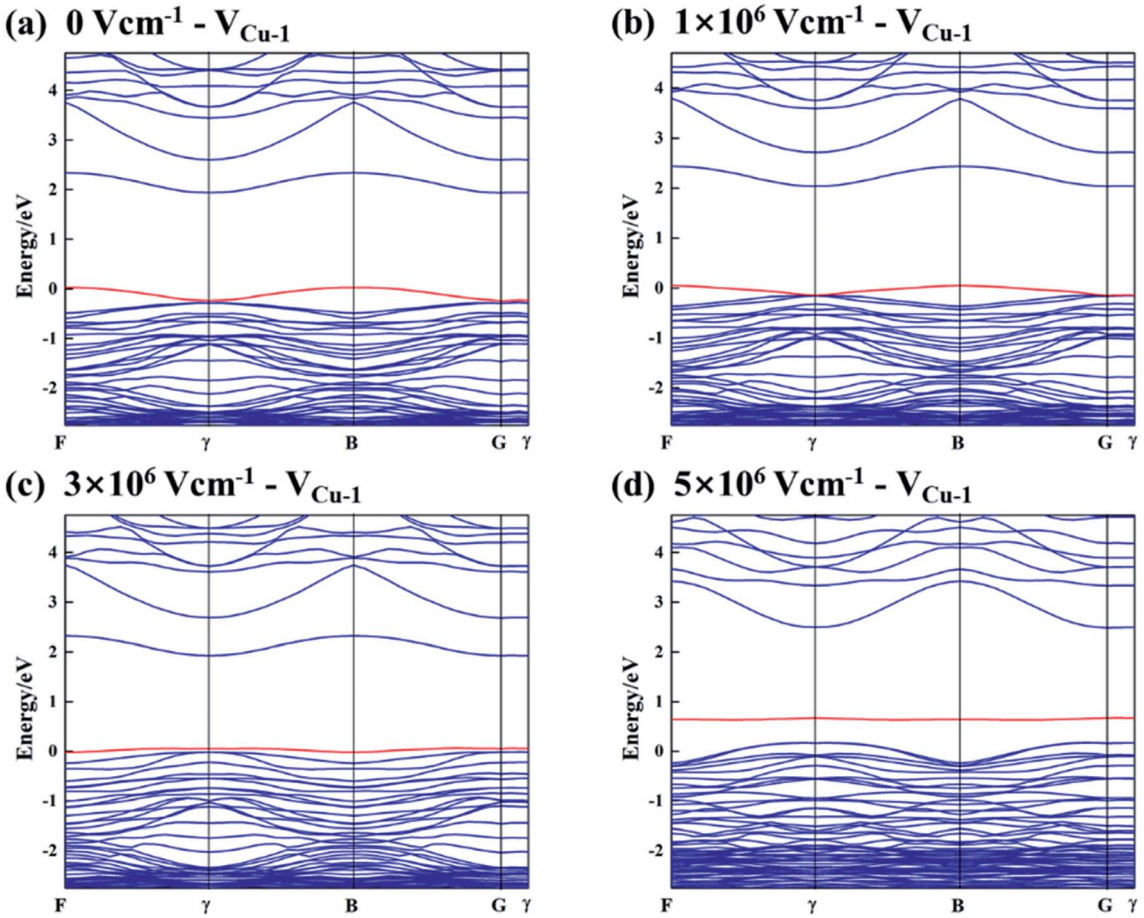

Fig. 3 Band structures of Cu_2O (111) with one $V_{Cu\text{-}1}$ under (a) 0, (b) 1, (c) 3 and (d) 5×10^6 V cm^{-1} electric field.

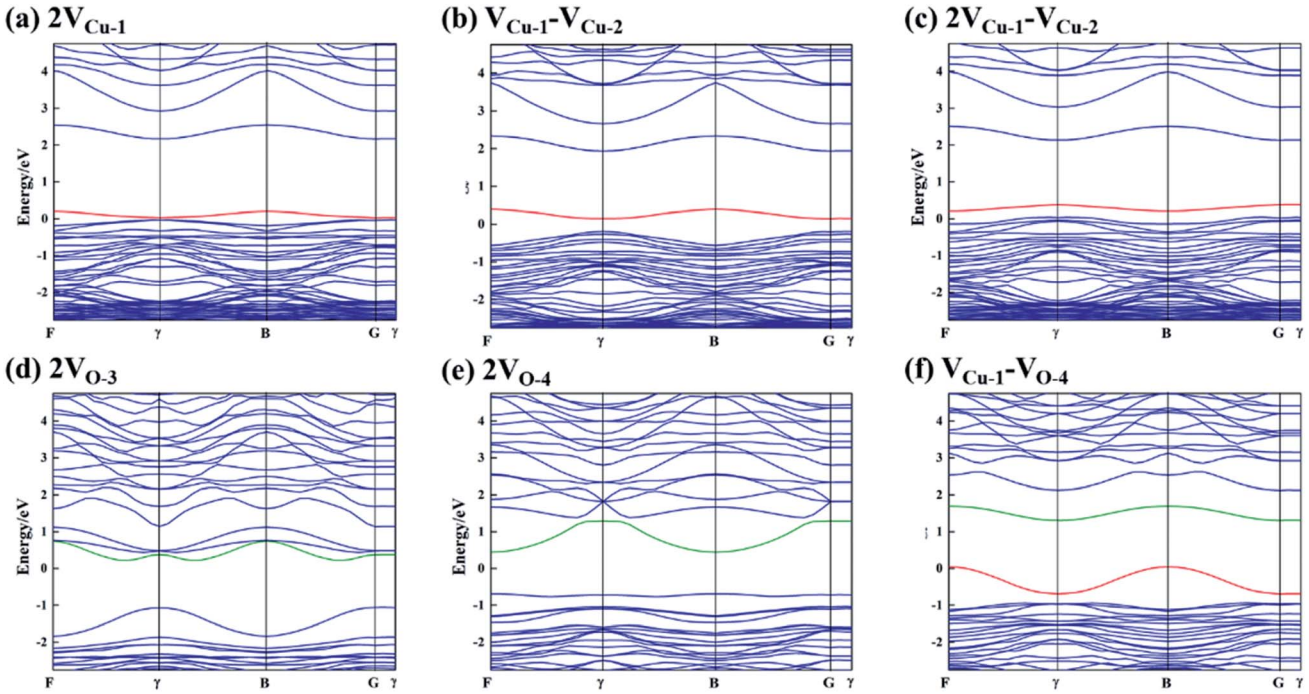

Fig. 4 Band structures of Cu_2O (111) with different concentrations of copper vacancies or oxygen vacancies.

concentration were calculated to indicate the effective role of a specific defect on band structure for oxide is not going to change due to varying concentration. The results were shown in Fig. 4. We improved the vacancy concentration by removing more cations or oxygen ions from Cu_2O (111) model. All of the band structures were obtained after relaxation calculations. From Fig. 4, it's clearly that the copper vacancy always can increase valence band maximum by introducing acceptor states in band gap no matter with any concentration of itself or oxygen vacancies. Similarly, the oxygen vacancy always cannot increase valence band maximum in any conditions. Thus, transplanting these results to passive film, only copper vacancy in bl could increase the VBM, while oxygen vacancy and chloride-occupied oxygen vacancy just result in a decrease in CBM.

Combining with experimental results where VBM increased significantly with introducing chloride into the electrolyte, a reasonable speculation could be concluded that an increase of copper vacancy concentration in passive film would be substantial indeed owing to the participation of chloride ions. This conclusion is coincidentally in agreement with the assumption of Point Defect Model (PDM). In PDM, the aggression process of chloride ions for passive film was described as chloride absorbs into surface oxygen vacancies at bl/outer layer (ol) interface and extract a cation in an autocatalytic process that leads to the continual generation of cation vacancies that are then migrate across the bl to condense at the metal/bl interface to separate the bl from substrate.

4. Summary and conclusions

In this paper, we investigated the band structure of the barrier layer of the passive film on copper in Cl-containing solutions by photo-electrochemical measurements and DFT calculations. The results were showed as follows:

(1) The band gap of passive film narrows with introducing chloride into the electrolyte, where VBM increased significantly from photo-electrochemical and UPS measurements.

(2) DFT calculations indicated that only copper vacancy in the oxide model could increase the VBM, while oxygen vacancy and chloride-occupied oxygen vacancy just result in a decrease in CBM.

(3) The combining results verified that an increase of copper vacancy concentration in passive film would be substantial indeed owing to the participation of chloride ions, which is consistent with the description of aggression role of Cl^- on the initial breakdown of passive film in PDM where Cl^- in solution could extract cation vacancy in the barrier layer of the passive film by interacting with a surface oxygen vacancy.

Conflicts of interest

There are no conflicts to declare.

Acknowledgements

This work was supported by the National Key Research and Development Program of China (No. 2017YFB0702300) and the National Natural Science Foundation of China (No. 51671029). Aoni Xu gratefully acknowledges the China Scholarship Council for supporting her stay at the University of California at Berkeley.

References

1 H. Lee and K. Nobe, Kinetics and mechanisms of Cu electrodissolution in chloride media, *J. Electrochem. Soc.*, 1986, **133**(10), 2035–2043.
2 E. D'Elia, O. E. Barcia, O. R. Mattos, N. Pébère and B. Tribollet, High-rate copper dissolution in hydrochloric acid solution, *J. Electrochem. Soc.*, 1996, **143**(3), 961–967.
3 M. A. Amin, K. Khaled, Q. Mohsen and H. Arida, A study of the inhibition of iron corrosion in HCl solutions by some amino acids, *Corros. Sci.*, 2010, **52**(5), 1684–1695.
4 M. Edwards, J. F. Ferguson and S. H. Reiber, The pitting corrosion of copper, *J. - Am. Water Works Assoc.*, 1994, **86**, 74–90.
5 G. Kear, B. Barker and F. Walsh, Electrochemical corrosion of unalloyed copper in chloride media–-a critical review, *Corros. Sci.*, 2004, **46**, 109–135.
6 S. Sathiyanarayanan, M. Sahre and W. Kautek, In-situ grazing incidence X-ray diffractometry observation of pitting corrosion of copper in chloride solutions, *Corros. Sci.*, 1999, **41**, 1899–1909.
7 C. Deslouis, B. Tribollet, G. Mengoli and M. M. Musiani, Electrochemical behaviour of copper in neutral aerated chloride solution. I. Steady-state investigation, *J. Appl. Electrochem.*, 1988, **18**, 374–383.
8 H. Strandberg and L. G. Johansson, Some aspects of the atmospheric corrosion of copper in the presence of sodium chloride, *J. Electrochem. Soc.*, 1998, **145**(4), 1093–1100.
9 X. Wei, C. Dong, P. Yi, A. Xu, Z. Chen and X. Li, Electrochemical measurements and atomistic simulations of Cl^--induced passivity breakdown on a Cu_2O film, *Corros. Sci.*, 2018, **136**, 119–128.
10 L. Lin, C. Chao and D. Macdonald, A point defect model for anodic passive films II. Chemical breakdown and pit initiation, *J. Electrochem. Soc.*, 1981, **128**, 1194–1198.
11 T. Dull, W. Frieze, D. Gidley, B. Scherer, D. Ellerbrock and D. Macdonald, Positron DBS studies of the corrosive breakdown of the passive film on titanium, in *Materials Science Forum*, Trans Tech Publ, 1997, vol. 255, pp. 671–673.
12 S. Ahn, H. Kwon and D. D. Macdonald, Role of chloride ion in passivity breakdown on iron and nickel, *J. Electrochem. Soc.*, 2005, **152**, B482–B490.
13 I. T. Fonseca, N. Lima, J. A. Rodrigues, M. I. S. Pereira, J. C. Salvador and M. G. Ferreira, Passivity breakdown of Al 2024-T3 alloy in chloride solutions: a test of the point defect model, *Electrochem. Commun.*, 2002, **4**, 353–357.
14 P. Zu, Z. Tang, G. K. Wong, M. Kawasaki, A. Ohtomo, H. Koinuma and Y. Segawa, Ultraviolet spontaneous and stimulated emissions from ZnO microcrystallite thin films at room temperature, *Solid State Commun.*, 1997, **103**, 459–463.
15 M. Abdel-Rahman, M. Abdallah and E. A. Badawi, Study of trapping rate and defect density in AlSi 11.35 Mg 0.23 by positron annihilation technique, *Surf. Rev. Lett.*, 2004, **11**, 427–432.
16 Y. Bai, Y. Ling, W. Lai, S. Xing and W. Ma, Electrochemical properties of the passive film on bulk Zr–Fe–Cr intermetallic fabricated by spark plasma sintering, *Appl. Surf. Sci.*, 2016, **388**, 212–222.
17 A. Fattah-Alhosseini, F. Soltani, F. Shirsalimi, B. Ezadi and N. Attarzadeh, The semiconducting properties of passive films formed on AISI 316 L and AISI 321 stainless steels: a test of the point defect model (PDM), *Corros. Sci.*, 2011, **53**, 3186–3192.
18 L. Jinlong, L. Tongxiang, W. Chen and D. Limin, Comparison of corrosion properties of passive films formed on coarse grained and ultrafine grained AISI 2205 duplex stainless steels, *J. Electroanal. Chem.*, 2015, **757**, 263–269.
19 L. Jinlong, L. Tongxiang, W. Chen and G. Ting, The passive film characteristics of several plastic deformation 2099 Al–Li alloy, *J. Alloys Compd.*, 2016, **662**, 143–149.
20 D. D. Macdonald, The passive state in our reactive metals-based civilization, *Arabian J. Sci. Eng.*, 2012, **37**, 1143–1185.
21 G. Paul, Y. Nawa, H. Sato, T. Sakurai and K. Akimoto, Defects in Cu_2O studied by deep level transient spectroscopy, *Appl. Phys. Lett.*, 2006, **88**, 141901.
22 H. Raebiger, S. Lany and A. Zunger, Origins of the p-type nature and cation deficiency in Cu_2O and related materials, *Phys. Rev. B: Condens. Matter Mater. Phys.*, 2007, **76**, 045209.
23 J. Heyd, G. E. Scuseria and M. Ernzerhof, Erratum: "hybrid functionals based on a screened Coulomb potential" [J. Chem. Phys., 118, 8207 (2003)], *J. Chem. Phys.*, 2006, **124**, 219906.
24 A. Xu, C. Dong, X. Wei, X. Li and D. D. Macdonald, DFT and photoelectrochemical studies of point defects in passive films on copper, *J. Electroanal. Chem.*, 2019, **834**, 216–222.
25 W. Jia, Z. Cao, L. Wang, J. Fu, X. Chi, W. Gao and L.-W. Wang, The analysis of a plane wave pseudopotential density functional theory code on a GPU machine, *Comput. Phys. Commun.*, 2013, **184**, 9–18.
26 W. Jia, J. Fu, Z. Cao, L. Wang, X. Chi, W. Gao and L.-W. Wang, Fast plane wave density functional theory molecular dynamics calculations on multi-GPU machines, *J. Comput. Phys.*, 2013, **251**, 102–115.
27 J. Tauc, Absorption edge and internal electric fields in amorphous semiconductors, *Mater. Res. Bull.*, 1970, **5**, 721–729.
28 U. Stimming, Photoelectrochemical studies of passive films, *Electrochim. Acta*, 1986, **31**, 415–429.
29 S. Lee, E. Cho, S. Ahn and H. Kwon, Photo-electrochemical analysis of the passive film on zircaloy-4, *Electrochim. Acta*, 2001, **46**, 2605–2611.
30 F. Caballero-Briones, A. Palacios-Padros, O. Calzadilla, I. d. P. Moreira and F. Sanz, Disruption of the chemical environment and electronic structure in p-type Cu_2O films by alkaline doping, *J. Phys. Chem. C*, 2012, **116**, 13524–13535.
31 J. Ghijsen, L. v. Tjeng, J. Van Elp, H. Eskes, J. Westerink, G. Sawatzky and M. Czyzyk, Electronic structure of Cu_2O and CuO, *Phys. Rev. B: Condens. Matter Mater. Phys.*, 1988, **38**, 11322.

32 H.-H. Strehblow, V. Maurice and P. Marcus, Initial and later stages of anodic oxide formation on Cu, chemical aspects, structure and electronic properties, *Electrochim. Acta*, 2001, **46**, 3755–3766.

33 A. Fattah-Alhosseini, O. Imantalab and F. R. Attarzadeh, Electrochemical Behavior of Nano-grained Pure Copper in Dilute Alkaline Solution with Chloride Ion Trace, *J. Mater. Eng. Perform.*, 2016, **25**, 4478–4483.

34 J. Kunze, V. Maurice, L. H. Klein, H.-H. Strehblow and P. Marcus, In situ STM study of the duplex passive films formed on Cu (1 1 1) and Cu (0 0 1) in 0.1 M NaOH, *Corros. Sci.*, 2004, **46**, 245–264.

35 M. Nolan and S. D. Elliott, The p-type conduction mechanism in Cu_2O: a first principles study, *Phys. Chem. Chem. Phys.*, 2006, **8**, 5350–5358.

36 A. Soon, X.-Y. Cui, B. Delley, S.-H. Wei and C. Stampfl, Native defect-induced multifarious magnetism in nonstoichiometric cuprous oxide: first-principles study of bulk and surface properties of Cu^{2-} δ O, *Phys. Rev. B: Condens. Matter Mater. Phys.*, 2009, **79**, 035205.